Characteristics and performances of the small and large field adaptive optics system AOC at the C2PU telescope

Lyu Abe, Olivier Lai, François-Xavier Schmider, Marcel Carbillet, Julien Dejonghe, Éric Aristidi, Benjamin Buralli, Frantz Martinache, Jean-Pierre Rivet, Farrokh Vakili

Characteristics and performances of the small and large field adaptive optics system AOC at the C2PU telescope

L. Abe, O. Lai, F.-X. Schmider, M. Carbillet, J. Dejonghe, É. Aristidi, B. Buralli, F. Martinache, J.-P. Rivet, and F. Vakili

Laboratoire Lagrange, Université Côte d'Azur/Observatoire de la Côte d'Azur/CNRS, Bât. Fizeau, Parc Valrose, 06100 Nice, France

ABSTRACT

AOC (Adaptive Optics system at Calern) is an adaptive optics bench being developed on the Epsilon (East) telescope of the two 1-m telescopes of C2PU (Centre Pédagogique Planète Univers), Calern observatory, Observatoire de la Côte d'Azur (OCA), near Nice (France). It is installed at the F/35 Coudé focus, and aims at correcting the wavefront in the visible and in the near-infrared, using an ALPAO 11x11 actuator-across deformable mirror feeding a 10x10 Shack-Hartmann wavefront sensor. It is currently being upgraded with a First Light Imaging OCAM2 EMCCD detector, which will allow us to increase the number of available pixels per sub-aperture and the loop frequency, as well as to take advantage from a negligible read-out.

The system is designed to work both in a standard stellar mode and in a more innovative planetary mode, capable of operating on planets such as Mars, Saturn and Jupiter, with a field up to 60 arcsec. Such a wide field is much larger than the isoplanatic angle, therefore only the turbulent ground layer can be corrected, up to an altitude of a few thousand meters. Extensive simulations have been carried out of these two different modes. The system is now undergoing implementation and validation using a low order modal control (10 to 16 modes), but a zonal control will be implemented next to ensure performance improvement down to $\lambda \sim 500$ nm. The loop frequency was limited to 500 Hz by the speed of the Andor iXon camera, but its replacement by an OCAM2 camera will allow to reach between 1.5 and 2.2 kHz (depending on binning). Theoretical performance of the system has been studied through simulations for the planetary mode and presented previously at SPIE.[1] Here we present the implementation of the system and its preliminary performance on the sky and comparison with the simulations.

In the future, we plan to better characterize the temporal transfer function as a function of the gain and the number of corrected modes, in order to implement an automatic gain control, both zonally in the visible and modally for near infrared applications. We are also implementing a control of the non-common path aberrations (NCPA). This is done by analysing the aberrations on a defocused stellar image, using the DONUT algorithm.[2] We intend to characterize these NCPA in real-time directly from the observations. We also consider parameterizing the resulting point-spread function from the real-time statistics of the adaptive optics system to be used for further data analysis.

Keywords: adaptive optics, wide-field sensing, planetary observation, numerical modelling

1. INTRODUCTION

The C2PU telescopes are twin 1-m diameter telescopes previously built for interferometry in the infrared,[3] and refurbished starting in 2010 with newly super-polished mirrors (polished at OCA). The goal was a multi-purpose usage, including astrophysical observations, training for students, AO research activities, and support for new optical concepts development and testing.

The Eastern telescope "Epsilon" is equipped with a Coudé focus in which an optical bench was installed to receive different instruments, including JOVIAL, an interferometric Doppler imager, specially designed for observations of planetary atmospheric dynamics.[4] Figure 1 shows the AOC bench design and the telescope Epsilon. Since 2014, the need for an adaptive optics (AO) system was envisioned, both to improve the quality of the images at the focal plane and to tests devices and methods in High Angular Resolution.[5] We will first summarize the characteristics of the system already described in[1] and describe the new configuration with a faster

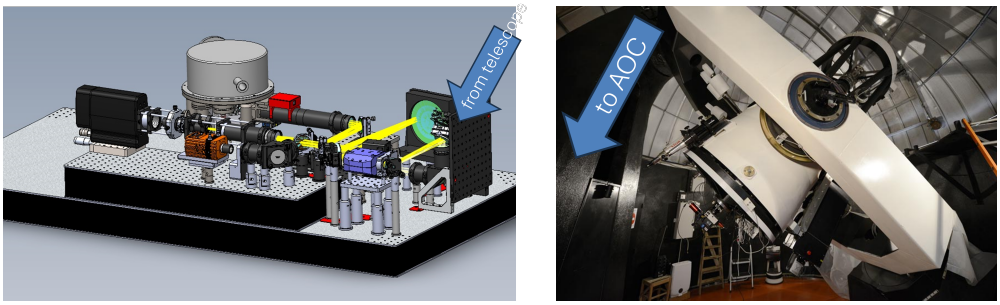

Figure 1. Left: Study view of the AOC design. Right: The 1m diameter Epsilon telescope.

WFS, allowing better performances. We show the result of different simulations with the new configuration for the stellar field mode and the planetary field mode. We then present preliminary temporal transfer functions recorded on the sky both on a star in the near infrared and on Jupiter in the visible domain. The measured transfer functions are in line with the estimated delay in the loop. In conclusion, we will present the perspectives of utilization and improvement of AOC.

2. SYSTEM DESCRIPTION

The AOC (AO at Calern) system was already described in.[1] In the present paper, we focus on the modifications to the optical design, the software and the main update of the wavefront sensor consisting in recently replacing the iXon-860 EMCCD with an OCAM2 EMCCD.

The system is designed to be of general use and needs to reach faint limiting magnitudes, for which low order modal control is ideally suited. The amplified OCAM2 EMCCD from First Light Imaging mitigates the read-out noise limitation in the case of faint objects observations. A validation of the capability to close the loop on stars up to magnitude 8 has been achieved so far, but this can be improved. In the visible, the main application is the observation of Jupiter, for which there is sufficient flux for a full-fledged zonal control.

The system uses an internal reference source, with both an unresolved object and an extended source for the planetary mode, for the calibration of the interaction matrix. The response of the AO correction can be calculated on the internal source in the same state of alignment as it is used on sky. To achieve this, AOC includes an active control of the pupil, both in position and rotation, as the field rotates at the Coudé focus. This is achieved thanks to a derotator module, placed at the entrance of the AO bench, and an active tip-tilt mirror placed at the focus of the Coudé train. The internal source includes a pupil shape which reproduces exactly the pupil of the telescope, including the asymmetric central obscuration and its spider arms. A motorized slider allows a fast switching between the internal source and the telescope field. This system proved to be very efficient for stability of the correction.

The OCAM2 camera offers 240×240 24-micron pixels which can be read-out at the maximum frame rate of 1503 Hz (665 microseconds), and can also work in 2×2 binned mode with an increased frame rate.

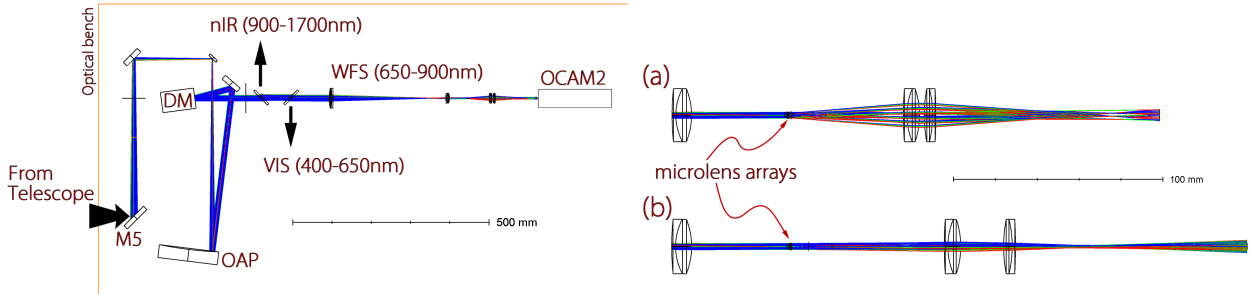

Figure 2. Left: AOC optical design. Right: Microlens array planetary (a) and stellar (b) optical configurations.

In the updated opto-mehanical setup, three configurations can be selected, with 3 different microlens arrays (MLA), all with a pitch of 300 μm, and focal lengths of 2, 5.1 and 18.8 mm, giving a sub-image field of view of 80.5 arcsec, 31 arcsec, and 8.5 arcsec, respectively. These are obviously intended to adapt to the stellar or planetary nature of the observed targets. The three configurations can be interchanged within minutes by changing the MLA support and re-imaging lenses as pre-configured assemblies, and resetting the camera position (optical configuration examples shown in Fig. 2). Focusing the WFS is ensured by displacement of the WFS mount by a quantity equal to the focal length of the MLA by means of calibrated spacers.

On the software side, AOC is driven by a parallelized C++ code for the main loop, in combination with a Python graphical user interface. The C++ multi-threaded loop code is running on a 14-cores Intel Xeon processor under Microsoft Windows 10 operating system. The loop itself runs with a timing of about 600 microseconds, for a maximum image frame rate of 1450 Hz. This means an average latency of about 1.5 frames, i.e. 900 microseconds, not accounting for the image transmission and deformable mirror (DM) command transmission delays (not currently known), and the DM settling time which is reported to be about 220 microseconds from the ALPAO DM97 test report. The python interface was originally designed by one of us (FM), inspired by the system used on Subaru/ScExAO using shared-memory buffers that allow fast communication and data transfer from the different software components (the original linux-specific C-code was ported to Windows). Several graphical tools allow the quick configuration of the active/inactive SH sub-images (with per-sub-image thresholds), the visualization of separate "DM aberration buffers" (low and high orders, as well as flat actuator and static aberrations maps). It is also possible to add static aberration modes during the correction in order to tune the PSFs on a given output port. An overview of the AOC GUI and its tools is shown in Fig. 3.

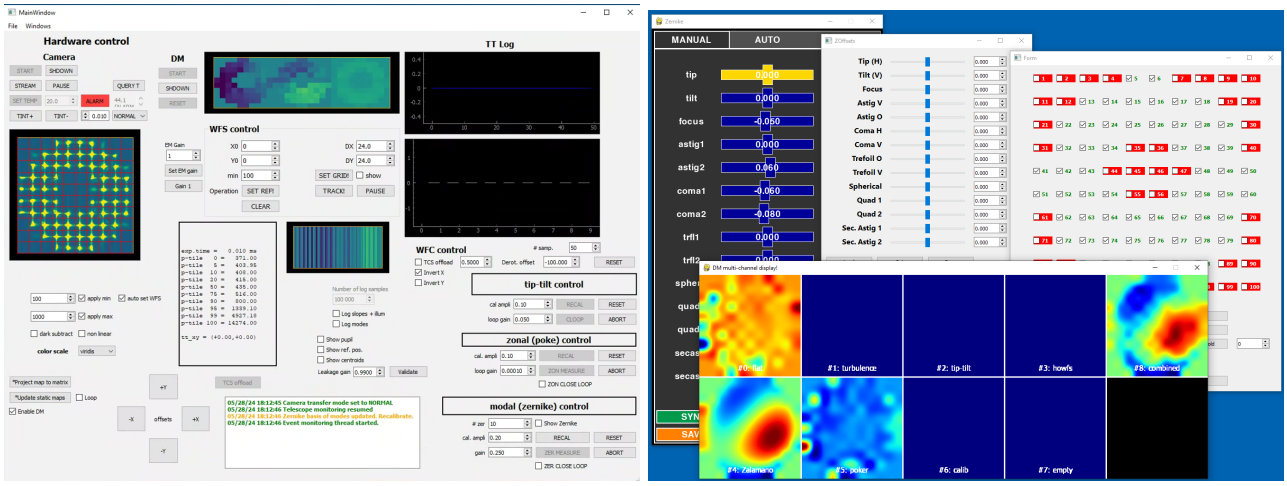

Figure 3. The AOC graphical user interface (under development). (Left) the main interface, and (Right) GUI tools.

3. SIMULATIONS

In this section, we show simulation results and performance obtained with the implementation of the new camera, comparing them with the performance provided with the previous iXon camera. Simulations were performed with two different end-to-end modelling tools, `CAOS`[6] and `instant_GLAO`,[7] which were used as a way to cross-validate the overall performance (since the codes are very different). We first simulated a two-layer (ground layer, free atmosphere) turbulence profile, the details of which are given in Table 1, together with the physical characteristics of the two version of the system considered.

Within this framework, we computed the residual wavefront error (rms) after modal correction of 14 Zernike modes as a function of the star magnitude, and compared the gain in performance provided by the OCAM2 WFS, shown in Fig. 4. Note that in full resolution mode, the OCAM2 camera can achieve 24×24 pixels per sub-aperture with a maximum achievable frame rate of 1.5 kHz, but a 2×2 binning is implemented here (leading to 12×12 pixels per sub-aperture), with a maximum theoretical frame rate of 2.2 kHz. One can note interesting

Table 1. Main parameters of the numerical simulations.

Turbulent atmosphere modelling	
Fried parameter r_0 (at 500 nm)	9.2 cm
number of turbulent layers	2
ground layer velocity	4 m/s
ground layer C_N^2 profile relative percentage	80%
high layer velocity	10 m/s
high layer C_N^2 profile relative percentage	20%
physical size of the turbulent layers	7+ m
wave-front outer-scale $\mathcal{L}_0$	27 m
simulation method	FFT-based, no sub-harmonics
AO guide star parameters	
spectral type	A0
V-magnitudes	0–14
Wavefront reconstruction and correction	
number of Zernike modes reconstructed	14
delay time	333,500 μs
Wavefront sensing modelling	
central sensing wavelength	700 nm
bandwidth	400 nm
total transmission	0.1
sub-aperture configuration	10×10
iXon CCD characteristics	
number of pixels per sub-aperture	12×12
pixel size	0.6 arcsec
⇒ sensing FoV	7.2 arcsec
exposure time (frequency)	2 ms (500 Hz)
OCAM EMCCD characteristics	
number of pixels per sub-aperture	12×12 & 24×24
pixel size	0.712 arcsec & 0.356 arcsec
⇒ sensing FoV	8.545 arcsec
exposure times (frequencies)	455 & 666 μs (2.2 & 1.5 kHz)
Wavefront control	
time-filter type	pure integrator
closed-loop gains	0.5–0.1

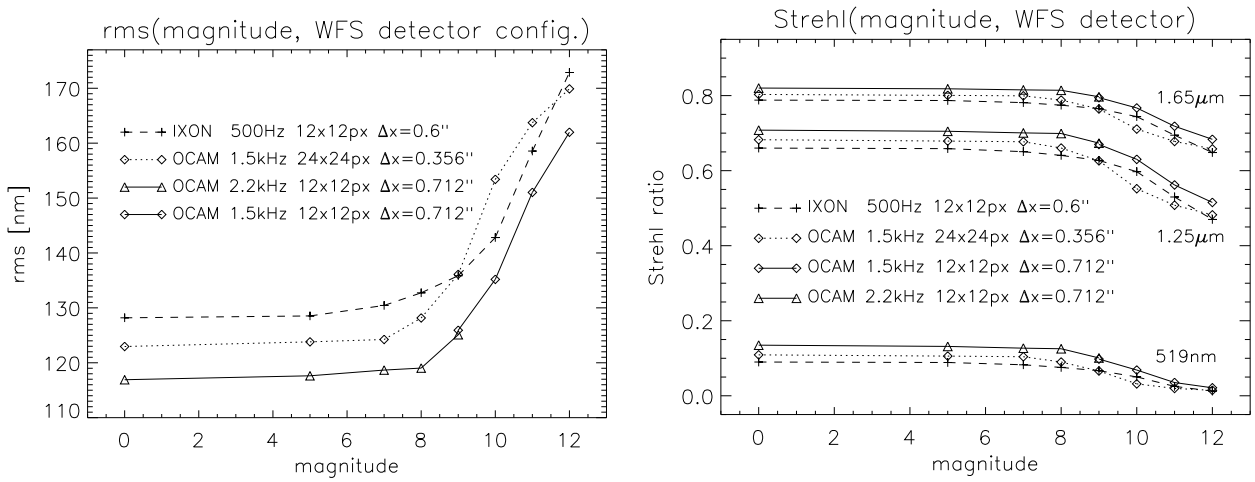

Figure 4. Left: the rms wavefront error in nm for our previous wavefront sensor camera, iXon, limited to 500 Hz maximum frame rate, and the OCAM2 camera, in binned mode. Right: the Strehl ratio at 519 nm, and in bands J and H (1.25 and 1.65 μm, respectively).

behaviors around magnitude 9. First, this is the point at which it becomes interesting to change the camera frequency, when using the OCAM2 camera. Optimal values are found to be 2.2kHz for guide stars brighter than magnitude 9, and 1.5 kHz for fainter stars. We only consider photon noise (neglecting read noise, also for the iXon) and this is also the point where the iXon is equivalent to the OCAM2 camera working with 24×24 pixels per sub-aperture. Below this magnitude, the OCAM2 is provides better performance while above, they become almost equivalent. Note that for the OCAM2, working at full sampling with 24×24 pixels per sub-aperture always provides better performance.

Figure 4 also shows the long exposure Strehl ratio, computed by means of the Maréchal approximation from the wavefront residual rms, for the J and H bands, as well as at 519 nm, the wavelength at which the zonal wind measurements are carried out with the JOVIAL instrument. A clear gain is visible with respect to the iXon detector working at 500 Hz, and a further gain is also found by increasing the sampling frequency from 1.5 kHz to 2.2 kHz. Not shown in this figure, we also found no difference between the un-binned 24×24 pixels per sub-aperture mode and the 12×12 pixels per sub-aperture mode if both are at 1.5 kHz, implying that the gain comes solely from reduced temporal error (the loop delay used in these simulations is 333μs, which has been found to be a little optimistic with respect to the measured loop delay on the bench).

Simulations were also carried out with the `instant_GLAO` software. Results are shown in Fig. 5, to compare performance between the stellar and planetary modes. These simulations do not show any difference in performance between the 24×24 pixels per sub-aperture mode and the 12×12 pixels per sub-aperture mode, assuming the highest achievable frame rate in each mode (1.5 kHz vs. 2.2 kHz); the source of this difference between the results coming from our two codes is not yet understood, but the overall performance as a function of magnitude is sufficiently close that the level of performance is quite convincing, given the very different code structures and implementations. For example, the `CAOS` simulations always use the highest possible frame rate, but the loop gain is lowered as the magnitude increases, while `instant_GLAO` requires the frame rate to be adjusted (as well as the loop gain) at high magnitudes to prevent loop instabilities. In all cases, a 5-second exposure PSF was simulated (corresponding to 11 000 iterations at 2.2 kHz, but only 250 iterations at 50 Hz). Another difference is that the long exposure PSF is computed in `instant_GLAO`, allowing to directly measure the full-width at half-maximum (FWHM) and the long exposure Strehl ratio.

With `instant_GLAO`, it is also possible to use Jupiter as a guide source; in its simplest implementation, the centroid is computed on either a uniform disk or an image of Jupiter, measuring 50 arcsec on sky, and with a magnitude of -2.7, which translates into 1.15×10^7 photons/integration time at 1.5 kHz over the pupil, which corresponds to the high flux regime. These results seem to indicate that the performance does not increase noticeably above 500 Hz sampling frequency, but this could be due to the fact that the modal correction only

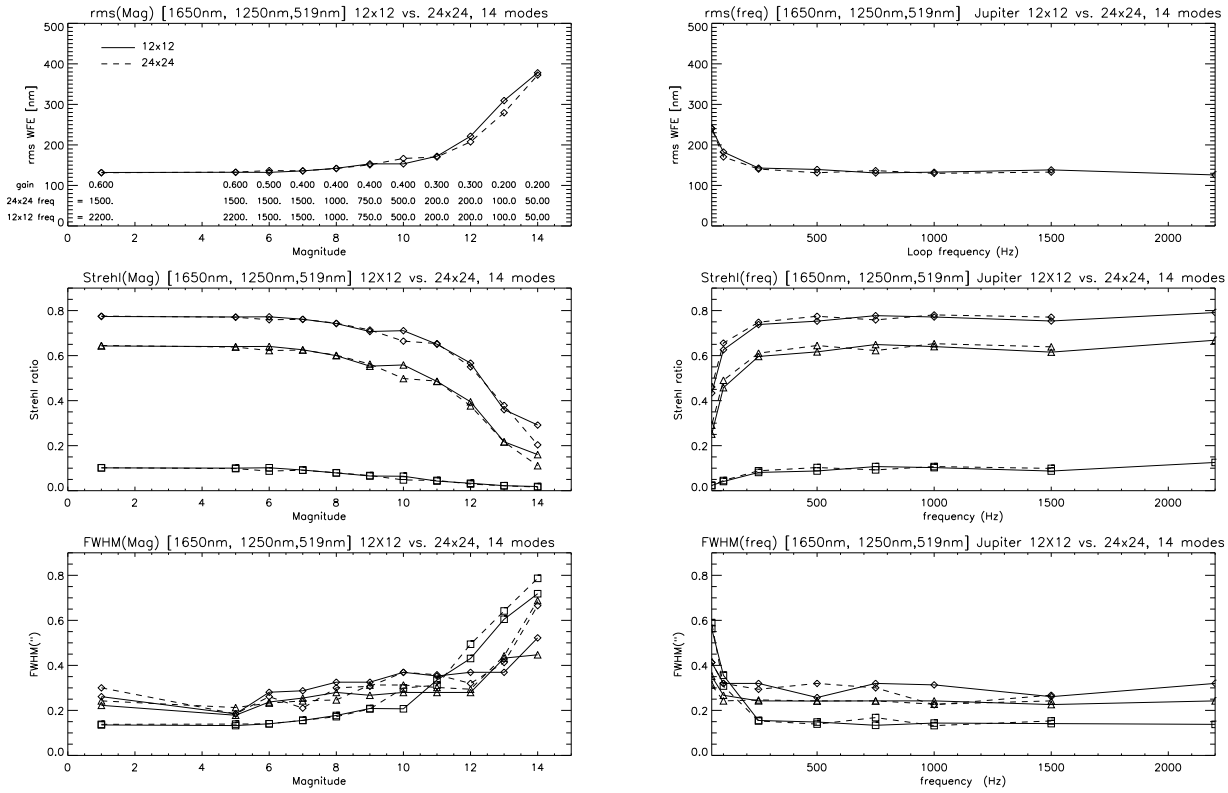

Figure 5. (Left) stellar mode performance as a function of magnitude. (Right) planetary mode using Jupiter as a guide source as a function of sampling frequency. There is no loss of performance on the bright end by using an extended, undersampled object for wavefront sensing.

includes the first 14 Zernike modes. We also note that in this configuration, no attempt is made to include the field averaging due to guiding on an extended source so these results correspond to the "on-axis" performance, which also probably explains why the performance of the planetary and stellar modes is so similar.

Its is possible to include the field averaging introduced by wavefront sensing on an extended object with `instant_GLAO`, by averaging multiple guide points across the disk of Jupiter. Using this feature, we can also study the image quality variation across the field. For these simulations, we used a zonal control to obtain the best possible performance at short wavelengths, as there is sufficient flux on Jupiter to operate at the highest sampling frequencies and still obtain more than 10^6 photons per subaperture and integration time. However, care had to be taken when using zonal correction, where the "petal" mode introduced between the top and bottom halves of the pupil, due to the M3 support structure which covers more than half of the width of a sub-aperture.

Results of these simulations are shown in Fig. 6, showing maps of FWHM and Strehl over a 2' field of view at 519 nm, J and H bands, using the average of 8 measurement points on the edge of the disk of Jupiter. The Strehl ratio in the visible is around 5%, and around 60% at H band, significantly lower than the 80% provided by the on-axis correction in modal control of Fig. 5, but this can be attributed to uncorrected high atmosphere turbulence. In the visible, with this optimistic correction, we can expect to achieve a resolution of 0.35" on the disk of Jupiter, a significant improvement from the starting 1" seeing ($r_0 = 9.2$cm).

4. PRELIMINARY ON-SKY RESULTS (PREVIOUS SYSTEM)

The current updated system could not yet be tested on-sky. With its previous configuration, AOC was used for observations of Jupiter in October 2023. The preliminary results of these observations are presented in[8] We present here results obtained with the AOC stellar field WFS using the iXon camera running at 500Hz with

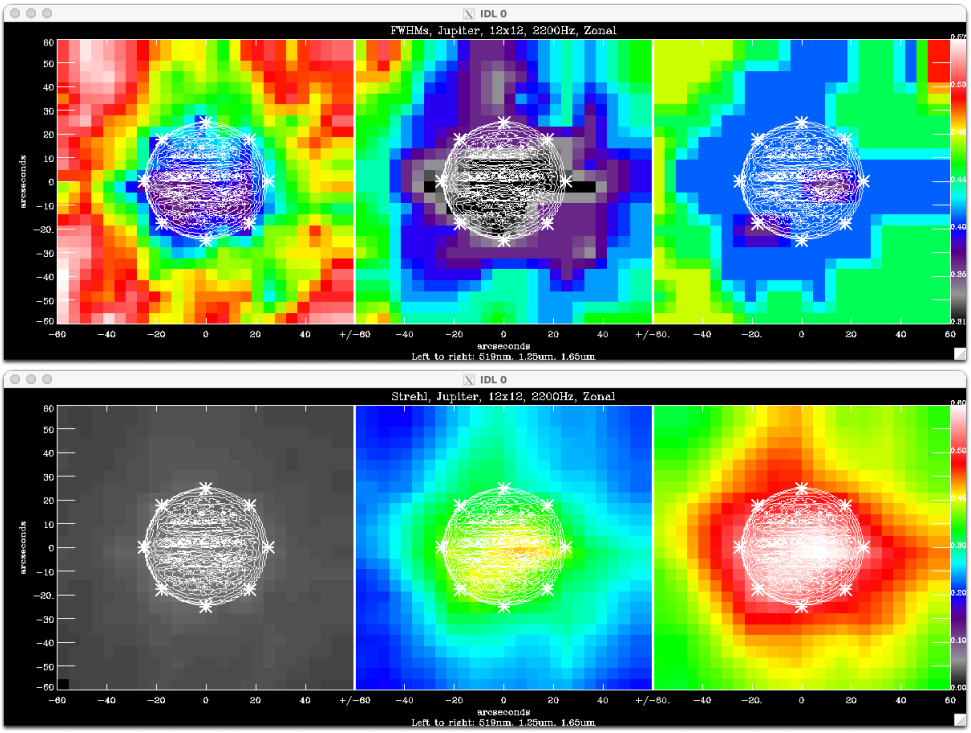

Figure 6. FWHM and Strehl obtained around a 2' field around Jupiter at 519nm, J and H bands, using the Calern turbulence profile, the average of 8 wavefront measurement in the locations of the white stars on the disk of Jupiter and a zonal cocntrol. In the visible (left), the Strehl ratio is around 5% and the FWHM around 0.35".

a moderate EMCCD gain. Figure 7 shows the results obtained on the G9III star β Lac (V=4.44, R=3.67, and H=2.21), recorded at the nIR focus with the Raptor Photonics Ninox camera equipped with an H-band filter. The continuous 57 s sequence containing 1000 frames was recorded with a 50ms exposure time. The frames were calibrated with a master dark composed of 1000×50ms frames. The AO system was alternately turned on and off during the recording (AO on, off, on, off, on) for a total of about 300 frames when the AO was off, and 700 frames with the AO turned on. The accumulated images with the AO turned off were computed as raw addition (left plot on Fig. 7) as well as with shift-and-add using the AstroImageJ software (middle plot), and then compared to the AO-compensated image that was simply the addition of all the AO-on images. The seeing conditions were quite good at that time (between 1∼1.5") so we clearly reach the near-diffraction limit on the AO-compensated images (0.32" at λ=1.6 μm). The calibration was done with the internal source, recalling that at that time, the pupil mask was not matching the actual telescope pupil (see above). This kind of result is very promising as the updated system will run with an effective loop speed at least twice as fast as in this example.

5. CONCLUSION

We have presented the AOC (Adaptive Optics at Calern) system and its improvements over the last few years, first on sky results as well as simulation results using two independent Monte Carlo simulation tools. AOC is an adaptive optics system developed to improve the spatial resolution needed for the study of the atmospheric dynamics of Jupiter using the JOVIAL instrument. But it is also a versatile teaching and development platform for new concepts in adaptive optics, despite its classical 10x10 SH wavefront sensor coupled to an 11x11 actuator DM in a Fried geometry. The wavefront sensor has three plate scales allowing to guide on extended solar system objects such as Jupiter, Saturn and Mars, and now uses an OCAM2 detector which provides sufficiently high frame rates for effective correction in the visible. The real-time code of the loop in C++ runs on a 14-cores Windows 10 operating system, for an effective loop timing (image trigger until DM command send) of 600 microseconds. It is combined with a Python graphical user interface and uses fast memory-shared buffers to exchange data, and several graphical tools to configure and control the system. We plan to include tools for

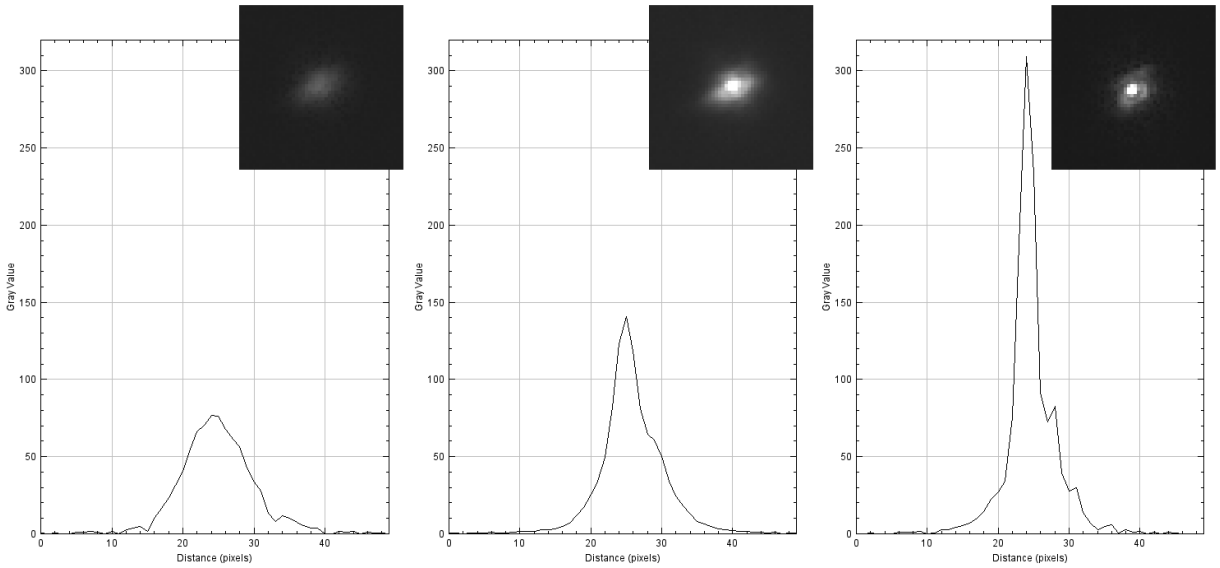

Figure 7. Observation of βLac on 20 July 2023 with the previous AOC configuration (iXon 888 @500Hz). (Left) horizontal line-cut of the raw accumulation of uncompensated images, (middle) with shift-and-add, and (right) with the AO system turned on (see text for details).

recording the performances of the AO system in real-time as a function of the parameters (gain, noise...) for optimisation of the control-loop and for a posteriori data processing. We already implemented some "PSF tuning" algorithms to minimize the Non Common Path Aberrations (NCPA) based on the analysis of the AO-corrected focal images, and we plan to make them more automatic.

Preliminary results on the sky both on stellar source and on planets[8] show performances conform to previous simulations.[1] Recent simulations of the new AOC configuration indicate that we should reach improved performance in the visible on Jupiter (on the order of 0.35"$\sim$0.4", and that the system should be capable of delivering high Strehl ratios (80% in modal control, $>90\%$ in full zonal control) in the near infrared. There are still discrepancies between the two codes in terms of optimal sampling frequency, loop gain and loop stability, but we are exploiting these differences to seek potential errors and to improve both codes until they match.

Thanks to its unique and flexible configuration, the AO system AOC installed on the Eastern telescope at C2PU will be able to offer excellent performances for many scientific programs in astrophysics and planetology and will be very useful to develop new instrumental concepts and data processing methods.

REFERENCES

[1] Buralli, B., Lai, O., Carbillet, M., Abe, L., Schmider, F. X., Dejonghe, J., Martinache, F., Aristidi, É., Cottalorda, É., Bresson, Y., Rivet, J. P., Vernet, D., and Vakili, F., "Numerical modelling of the planetary adaptive optics mode of AOC, the adaptive optics project at Calern Observatory," in [*Adaptive Optics Systems VIII*], Schreiber, L., Schmidt, D., and Vernet, E., eds., *Society of Photo-Optical Instrumentation Engineers (SPIE) Conference Series* **12185**, 121858R (Aug. 2022).

[2] Tokovinin, A. and Heathcote, S., "Donut: Measuring Optical Aberrations from a Single Extrafocal Image," *PASP* **118**, 1165–1175 (Aug. 2006).

[3] Gay, J. and Rabbia, Y., "Heterodyne Interferometry in InfraRed at OCA-Calern Observatory in the seventies," in [*Improving the Performances of Current Optical Interferometers & Future Designs*], Arnold, L., Le Coroller, H., and Surdej, J., eds., 181–189 (Apr. 2014).

[4] Gonçalves, I., Schmider, F.-X., Bresson, Y., Dejonghe, J., Preis, O., Robbe-Dubois, S., Appourchaux, T., Boumier, P., Leclec'h, J.-C., Morinaud, G., Gaulme, P., and Jackiewicz, J., "Advances in the development of a Mach-Zehnder interferometric Doppler imager for seismology of giant planets," in [*Ground-based and*

Airborne Instrumentation for Astronomy VI], Evans, C. J., Simard, L., and Takami, H., eds., *Society of Photo-Optical Instrumentation Engineers (SPIE) Conference Series* **9908**, 99083M (Aug. 2016).

[5] "HiPIC (High angular resolution Post-adaptive optics Imaging at Calern observatory)." https://www.oca.eu/fr/lag-mpo-prog.

[6] Carbillet, M., Vérinaud, C., Femenía, B., Riccardi, A., and Fini, L., "Modelling astronomical adaptive optics - I. The software package caos," *Monthly Notices of the Royal Astronomical Society* **356**, 1263–1275 (02 2005).

[7] Lai, O., Chun, M. R., Pazder, J., Véran, J.-P., Jolissaint, L., Andersen, D., Salmon, D., and Cuillandre, J.-C., "Imaka: a lagrange invariant of ELTs," in [*Adaptive Optics Systems II*], Ellerbroek, B. L., Hart, M., Hubin, N., and Wizinowich, P. L., eds., **7736**, 77361D, International Society for Optics and Photonics, SPIE (2010).

[8] Schmider, F.-X., Gaulme, P., Abe, L., Dejonghe, J., Lai, O., Carbillet, M., Rivet, J.-P., Gonçalves, Y., and Jackiewicz, J., "Improvement of Doppler measurements thanks to adaptive optics: the case of JOVIAL+AOC," in [*Adaptive Optics Systems IX*], *Society of Photo-Optical Instrumentation Engineers (SPIE) Conference Series* **13097** (2024).